Air-Induced Passive Intermodulation in FDD Networks: Modeling, Cancellation and Measurements

Vesa Lampu*, Lauri Anttila*, Matias Turunen*, Marko Fleischer†, Jan Hellmann†, and Mikko Valkama*
*Department of Electrical Engineering, Tampere University, 33720 Tampere, Finland
†Nokia Mobile Networks, D-89081 Ulm, Germany
E-mail: vesa.lampu@tuni.fi

***Abstract*—In this paper, we consider the effects of air-induced passive intermodulation (PIM) in frequency division duplexing (FDD) transceiver systems. Specifically, we are focusing on the issue in multiantenna frequency range 1 (FR-1) base station (BS) systems. The air-induced PIM is a special case of intermodulation distortion, which stems from metallic objects within the radiation pattern of the transceiver system, due to so-called "rusty bolt" effect, where the induced nonlinear distortion is reflected back to the receiver. In order to cancel the received PIM, we develop a model for the perceived interference at the receiver of the BS and utilize the model to produce an estimate of the PIM signal, and to suppress it from the received data. To verify the proposed air-PIM modeling and cancellation scheme, extensive experimentation is carried out with an FDD capable transceiver system at NR band n3. The experiments show great promise in the achievable PIM cancellation levels, as the received air-induced PIM can be suppressed by more than 20 dB with the developed digital cancellation solution.**

***Index Terms*—Passive intermodulation, rusty-bolt, nonlinear distortion, digital cancellation**

I. Introduction

In order to increase the throughput and capacity of wireless systems in 5G NR [1], it is possible to flexibly allocate spectral resources from different channels and bands through carrier aggregation (CA), either utilizing the spectrum contiguously or non-contiguously. Additionally, 5G NR specifies the use of frequency-division duplexing (FDD) for certain frequency range (FR)-1 bands, as was the case in long-term evolution (LTE). In FDD, the transmitter (TX) and receiver (RX) operate simultaneously on different frequencies, and it is common for an operator to have a non-contiguous frequency allocations. These factors account for the rise of intermodulation (IM) distortion in the receiver frequencies of such bands, e.g., 5G NR band n3 (Band 3 in 4G/LTE), where RX bands lie on frequencies of the possible intermodulation products of the aggregated carriers, when utilizing the spectrum non-contiguously.

Intermodulation products are generated on the intermodulation frequencies when two or more carriers at different frequencies experience a common nonlinear distortion [2], such as can be the case in non-contiguous CA. In the TX chain, the most notable source of nonlinearity is the power amplifier (PA), which can be shared by the component carriers (CCs). Passive devices, such as connectors in the TX chain, can also act as nonlinearity sources [3], [4]. In these cases, the generated IM is referred to as passive intermodulation (PIM).

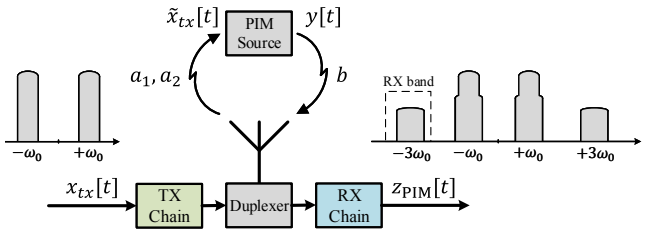

Fig. 1. Considered simplified system model where an external nonlinear passive device generates passive intermodulation to the receiver band, with the relevant signals shown.

No matter the source, the IM distortion is powerful interference from the receiver's perspective, if the IM products fall on the RX frequencies, possibly causing desensitization. While it is possible to mitigate the IM distortion issue by backing off the TX power or utilizing linear devices, these decrease the power efficiency and increase the production costs of devices, respectively. Alternatively, the IM distortion can be suppressed using digital canceller techniques. The shared PA induced IM distortion is modeled and cancelled e.g. in [2], [5]–[7]. It is also possible to employ digital predistortion (DPD) techniques to linearize the shared nonlinearity output, thus also mitigating the IM distortion [8]. Meanwhile, works such as [9], [10] concentrate on modeling and cancelling PIM specifically.

Often the source of PIM is within the transmitter hardware, but it is also possible for passive devices in the radiation field of the TX antennas to act as PIM sources, giving rise to air-induced PIM. This so-called "rusty-bolt" effect has been reported in literature [11], [12], but to the best of the authors' knowledge, no works besides [13] consider the digital cancellation of the air-induced PIM specifically. In light of this, in this paper we present a model for a system where air-induced PIM is being generated, and based on the model, digital cancellation solutions are developed. Based on cancellation results from measured data, we show that it is possible to mitigate the air-induced PIM issue with digital cancellation.

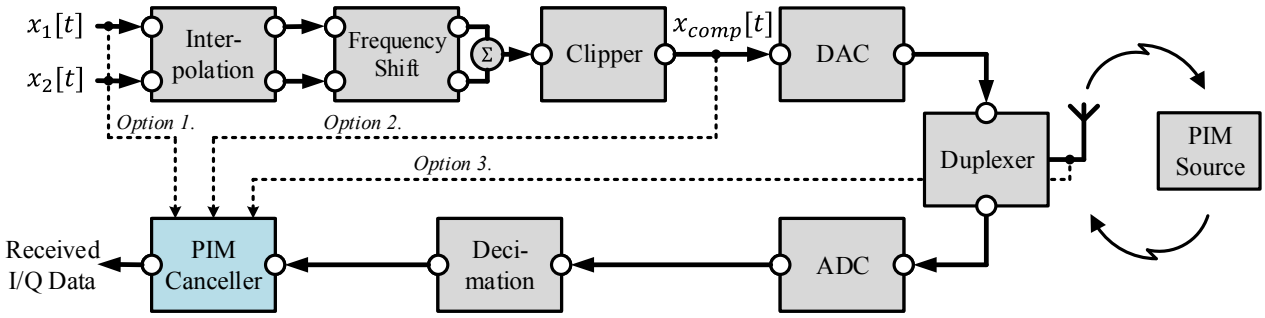

Fig. 2. Block diagram of the transceiver system illustrating the relevant blocks for the PIM canceller. Three possible points where to take the TX signal information are identified, where *Option 1.* corresponds to utilizing the baseband signals, *Option 2.* using the aggregated, clipped and oversampled composite signal and *Option 3.* measuring the TX signal from the antenna output.

II. System Model

A simplified diagram of the system model is presented in Fig. 1. We consider a transceiver system, comprised of a single TX chain serving a directional antenna array and a PIM source in the radiation field of the antennas. The transmitter utilizes CA, and the transmitted signal $x_{tx}[t]$ at baseband can be defined as

$$x_{tx}[t] = x_1[t]e^{-j\omega_0 t} + x_2[t]e^{+j\omega_0 t}, \tag{1}$$

where $x_1[t]$ and $x_2[t]$ represent the individual transmitted CC time domain baseband signals and ω_0 denotes the frequency offset of the carriers from zero frequency. For modeling purposes, we omit all possible TX chain impairments, such as PA nonlinearity and I/Q imbalance of the mixing stage.

The signal $x_{tx}[t]$ then propagates through an air channel to the PIM source. Assuming a pure line-of-sight (LOS) channel between the TX antennas and the PIM source and a frequency flat response within the signal bands, the channel can be modeled simply with two complex coefficients a_1 and a_2, which weigh the two component carriers separately. Then, the signal at the PIM source input $\tilde{x}_{tx}[t]$ can be written as

$$\tilde{x}_{tx}[t] = a_1 x_1[t]e^{-j\omega_0 t} + a_2 x_2[t]e^{+j\omega_0 t}. \tag{2}$$

The PIM source acts as a nonlinear device, thus causing nonlinear distortion on the input signal. Utilizing a generalized memory polynomial (GMP) model [14], a subset of the Volterra series, for the nonlinear behavior, the PIM source output signal $y[t]$ can then be generally written as

$$y[t] = \sum_{m=-M_1}^{M_2} \sum_{k\in K} \sum_{\substack{p=1 \\ p \text{ odd}}}^{P} g_{mkp}\tilde{x}_{tx}[t-m]|\tilde{x}_{tx}[t-m-k]|^{p-1} \tag{3}$$

where M_1 and M_2 are the number of precursor and postcursor taps, respectively, $K = \{-k_K \cdots - k_1\ k_1 \cdots k_K\}$ is a set of the considered amounts of lead and lag in envelope samples, P is the polynomial order of the nonlinearity and g_{mkp} are the complex coefficients of each nonlinearity term. For simplicity of expressions, the same number of memory taps for each envelope lead and lag and each nonlinearity order is considered here.

Again utilizing the same assumptions as before for the channel between the PIM source and the transceiver, the nonlinear signal $y[t]$ is reflected to the RX chain, undergoing a simple magnitude transform and phase shift. The received signal $z_{\text{PIM}}[t]$ over the whole band can then be determined as

$$z_{\text{PIM}}[t] = by[t], \tag{4}$$

where b is the channel coefficient from the PIM source to the RX chain. Here, we choose to model the IMD3-, i.e., the lower third order intermodulation product, which appears at frequency $-3\omega_0$, assuming all the other signal parts are filtered out perfectly. The filtered signal falling to this frequency up to fifth nonlinearity order ($P = 5$) can be written as

$$\begin{aligned} z_{\text{PIM,RX}}[t] = be^{j2\omega_0 k}\Bigg(& \sum_{m=-M_1}^{M_2} \sum_{k\in K} \big(g_{m,k,3}a_1^2 a_2^* \\ & \times x_1[t-m]x_1[t-m-k]x_2^*[t-m-k] \\ & + g_{m,k,5}a_1^2 a_2^* |a_1|^2 \\ & \times x_1[t-m]x_1[t-m-k]x_2^*[t-m]|x_1[t-m-k]|^2 \\ & + g_{m,k,5}a_1^2 a_2^* |a_2|^2 \\ & \times x_1[t-m]x_1[t-m-k]x_2^*[t-m]|x_2[t-m-k]|^2 \\ & + \cdots\big)\Bigg) \end{aligned} \tag{5}$$

from where we can identify the basis functions (BFs) of the IMD3- model. It can be seen that each BF consists of signals $x_1[t]$ and $x_2[t]$, with various combinations of delays between the signals. The expression can be simplified by lumping the

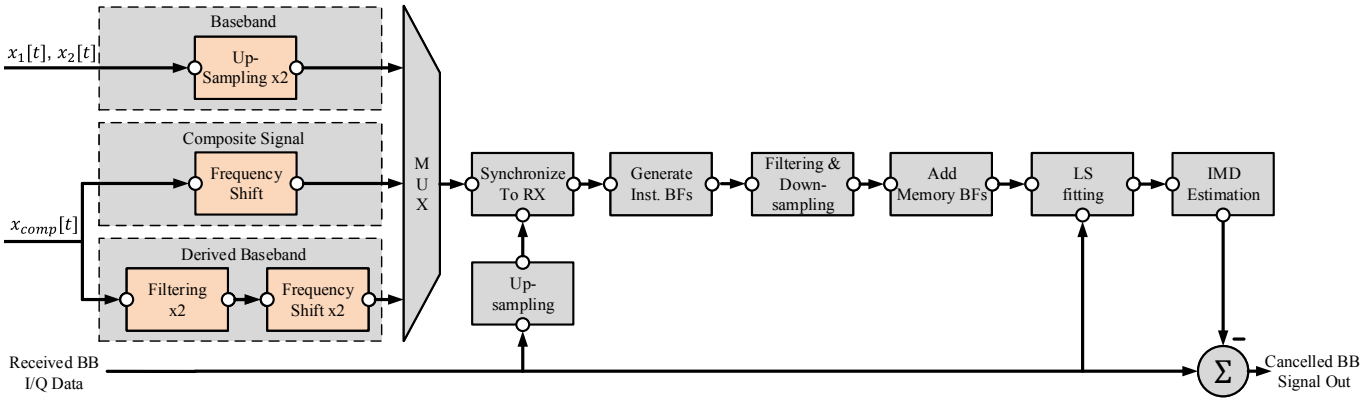

Fig. 3. Block diagram presentation of the digital PIM canceller, with the differences between the three considered solutions highlighted.

complex coefficients as

$$
\begin{aligned}
&z_{\mathrm{PIM,RX}}[t] = \\
&\sum_{m=-M_1}^{M_2} \sum_{k\in K} \big(c_{1,m,k} x_1[t-m] x_1[t-m-k] x_2^*[t-m-k] \\
&+ c_{2,m,k} x_1[t-m] x_1[t-m-k] x_2^*[t-m] |x_1[t-m-k]|^2 \\
&+ c_{3,m,k} x_1[t-m] x_1[t-m-k] x_2^*[t-m] |x_2[t-m-k]|^2 \\
&+ \cdots \big) \qquad (6) \\
&= \sum_{m=-M_1}^{M_2} \sum_{k\in K} \big(c_{1,m,k} \phi_{1,k}[t-m] \\
&+ c_{2,m,k} \phi_{2,k}[t-m] \\
&+ c_{3,m,k} \phi_{3,k}[t-m] \\
&+ \cdots \big) \qquad (7)
\end{aligned}
$$

where c are the lumped, total coefficients of each BF $\phi_{n,m,k}$. Based on the received signal model, the PIM signal can be predicted when the coefficients c are known.

III. Canceller Solutions

Stemming from the presented system model, we introduce three canceller solutions for suppressing the received PIM in this section. Each canceller aims to model the received PIM signal based on the knowledge of the transmitted and received signals by identifying the BF coefficients. The difference of the cancellers lies in where the transmitted signals are taken from in the TX chain, which subsequently affects how the signals are treated before the BF generation and how the BFs are generated within the PIM cancellation stage. Fig. 2 illustrates the transceiver system and possible points where to take the transmitted signal data to the PIM canceller. Here, we consider three canceller models, based on *Option 1.* and *Option 2.* in Fig. 2. We also note *Option 3.* in Fig. 2, i.e., measuring the antenna output signal as an alternative for the transmitted signal data acquisition, however, this option is omitted in this work, as the measurement of the antenna signals requires dedicated additional equipment, increasing the complexity of the overall system. Moreover, the modeling in this case is similar to the two latter presented cancellers in the following subsections, the main benefit of *Option 3.* being the inclusion of all TX chain effects in the data, even ones omitted in Fig. 2, such as PA nonlinearity and digital predistortion.

Each canceller solution utilizes least squares (LS) fitting to identify the BF coefficients c, which can be written as

$$\hat{\mathbf{c}} = (\mathbf{\Phi}^H \mathbf{\Phi})^{-1} \mathbf{\Phi}^H \mathbf{z}_{\mathrm{PIM,RX}}, \qquad (8)$$

where $\hat{\mathbf{c}}$ represents a vector of the estimated BF coefficients c, $\mathbf{\Phi}$ is the BF matrix, where each BF vector occupies a single column of the matrix and $\mathbf{z}_{\mathrm{PIM,RX}}$ is the received PIM signal as a column vector. Then, using the estimated BF coefficients $\hat{\mathbf{c}}$, a prediction of the PIM signal can be made with the next batch of data and the predicted signal is simply subtracted from the received data, as

$$\mathbf{z}_{\mathrm{RX}} = \mathbf{z}_{\mathrm{PIM,RX}} - \mathbf{\Phi}\hat{\mathbf{c}}, \qquad (9)$$

where the PIM distortion is suppressed in the signal $\mathbf{z}_{\mathrm{RX}}$.

Fig. 3 illustrates the PIM canceller procedure, highlighting the differences in signal processing in the three considered models in the beginning. After this stage, the signal or signals are synchronized with the upsampled RX data, by determining the cross-correlation between the third order BF $x_1^2 x_2^*$ and the RX data. Utilizing a high oversampling ratio will produce subsample delays at the original sample rate, which do not significantly affect the modeling capability. After the synchronization, the instantaneous ($m = 0$) BFs are generated, using the considered values for P and K. The instantaneous BFs thus incorporate also the leading and lagging envelope terms. Since the BFs have larger bandwidths than the original signals, oversampling is required to avoid aliasing. Therefore, the BFs have to be consequently filtered and downsampled after generation. Memory is applied to the model after downsampling by introducing leading and lagging copies of the generated instantaneous BF signals. Finally, LS fitting is used to determine the BF coefficients after (8) and the prediction and cancellation are performed after (9).

TABLE I
COMPARISON OF THE MERITS AND DRAWBACKS OF THE PRESENTED CANCELLER SOLUTIONS.

Model	Baseband	Composite	Derived Baseband
Pros	Simple processing	TX chain effects considered	TX chain effects considered
	Does not require high oversampling for BFs	Least BFs per given order	Does not require high oversampling for BFs
Cons	TX chain effects not considered	Highest required oversampling	Most complex processing

A. Baseband (BB) Canceller

Arguably the most straightforward way to obtain the transmitted signal data is to use the baseband signals $x_1[t]$ and $x_2[t]$, labeled as *Option 1.* in Fig. 2. In Fig. 3 it can be seen that these signals require upsampling to BF generation rate. Since this canceller model deals with the baseband representations of the signals, the BF matrix row for the BB canceller $\mathbf{\Phi}_{\mathrm{BB}}$ at time instance t can be defined as

$$\mathbf{\Phi}_{\mathrm{BB}}[t] = \big[\boldsymbol{\phi}_1[t+M_1] \ \cdots \ \boldsymbol{\phi}_1[t-M_2] \, \boldsymbol{\phi}_2[t+M_1] \ \cdots\big], \tag{10}$$

where the row vector $\boldsymbol{\phi}_n[t]$ is defined as

$$\boldsymbol{\phi}_n[t] = \big[\phi_{n,k_1}[t] \ \cdots \ \phi_{n,k_K}[t]\big]. \tag{11}$$

The complete matrix $\mathbf{\Phi}_{\mathrm{BB}}$ is then obtained by letting t run for L cycles, where L is the considered signal length and stacking the rows. The index k runs through the considered lead/lag of the envelope.

Since the input signals are the pure generated baseband signals, they lack information about the possible TX chain effects, most notable of which in our system is the clipper, which is also shown in Fig. 2. Therefore, the inputs $x_1[t]$ and $x_2[t]$ do not perfectly model the signals that are actually transmitted, hindering the cancellation performance.

B. Composite Signal (Comp) Canceller

To circumvent the abovementioned modeling issue of the baseband signals, an alternative is to input the *composite* signal $x_{comp}[t]$ to the PIM canceller, as is noted with *Option 2.* in Fig. 2. The composite signal contains both signals $x_1[t]$ and $x_2[t]$, shifted to an intermediate frequencies of $-\omega_0$ and ω_0, respectively, as $x_{comp}[t] = x_1[t]e^{-j\omega_0 t} + x_2[t]e^{+j\omega_0 t}$ with high oversampling. Thus, in the canceller, the composite signal is frequency shifted by $+3\omega_0$, as is shown in Fig. 3 to produce $\tilde{x}_{comp}[t]$, since the IMD3- BFs lie at frequency $-3\omega_0$. Since $\tilde{x}_{comp}[t]$ is a single signal, the BFs can be written using only this, following Equations (3) and (4), which reduces the number of BFs in the system. Then the BF matrix row at time instant t for the Comp canceller $\mathbf{\Phi}_{\mathrm{Comp}}$ can be defined as

$$\mathbf{\Phi}_{\mathrm{Comp}}[t] = \big[\boldsymbol{\varphi}_3[t-M_1] \ \cdots \ \boldsymbol{\varphi}_3[t+M_2] \, \boldsymbol{\varphi}_5[t-M_1] \ \cdots\big], \tag{12}$$

where the row vector $\boldsymbol{\varphi}_p[t]$ is defined as

$$\boldsymbol{\varphi}_p[t] = \begin{bmatrix} \mathrm{LPF}\{\tilde{x}_{comp}[t]|\tilde{x}_{comp}[t-k_1]|^{p-1}\} \\ \vdots \\ \mathrm{LPF}\{\tilde{x}_{comp}[t]|\tilde{x}_{comp}[t-k_K]|^{p-1}\} \end{bmatrix}^T, \tag{13}$$

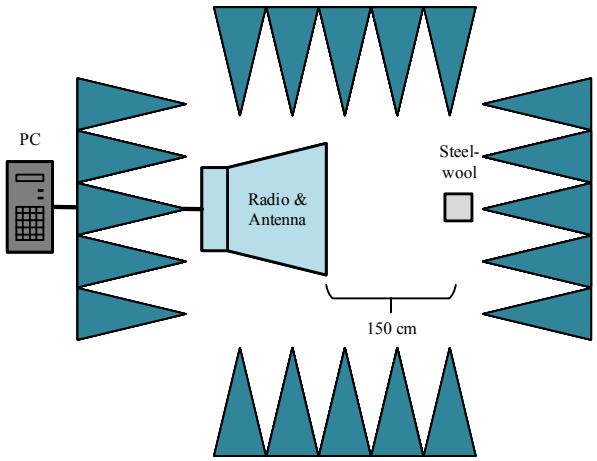

Fig. 4. Simplified model of the measurement setup. The BS, consisting of radio and antenna, is placed in an anechoic chamber with steel wool, and controlled by a PC from outside the chamber.

where $\mathrm{LPF}\{\cdot\}$ indicates a low-pass filtering operation, and the index p runs as in Equation (3). The matrix $\mathbf{\Phi}_{\mathrm{Comp}}$ is also generated by letting t run for L cycles and stacking the rows.

Following Equations (3) and (5), it can be seen that $\mathbf{\Phi}_{\mathrm{Comp}}$ is equivalent with $\mathbf{\Phi}_{\mathrm{BB}}$ when considering the signals of $\mathbf{\Phi}_{\mathrm{Comp}}$ at $-3\omega_0$, however, for a given BF order above three, $\mathbf{\Phi}_{\mathrm{Comp}}$ requires less BFs. Yet, the generation stage of $\mathbf{\Phi}_{\mathrm{Comp}}$ contains also the carrier information, which is filtered when the BFs are downsampled, but due to this, the oversampling requirement for the BF generation is higher than in the BB canceller, which increases the computational load of the composite signal canceller.

C. Derived Baseband (Der BB) Canceller

In order to avoid the high oversampling requirement in the BF generation, the composite signal may be used to derive the signals $x_1[t]$ and $x_2[t]$, while still including the effects of the clipper and other RX chain effects up to that point. Fig. 3 shows the required blocks to achieve this in the Derived baseband case: the signal needs to be filtered and frequency shifted twice to derive the individual signals $x_1[t]$ and $x_2[t]$ from $x_{comp}[t]$. The added complexity from the signal separation task is the obvious downside of the Der BB canceller. Otherwise the canceller is identical to the BB canceller, the instantaneous BF matrix for the Der BB

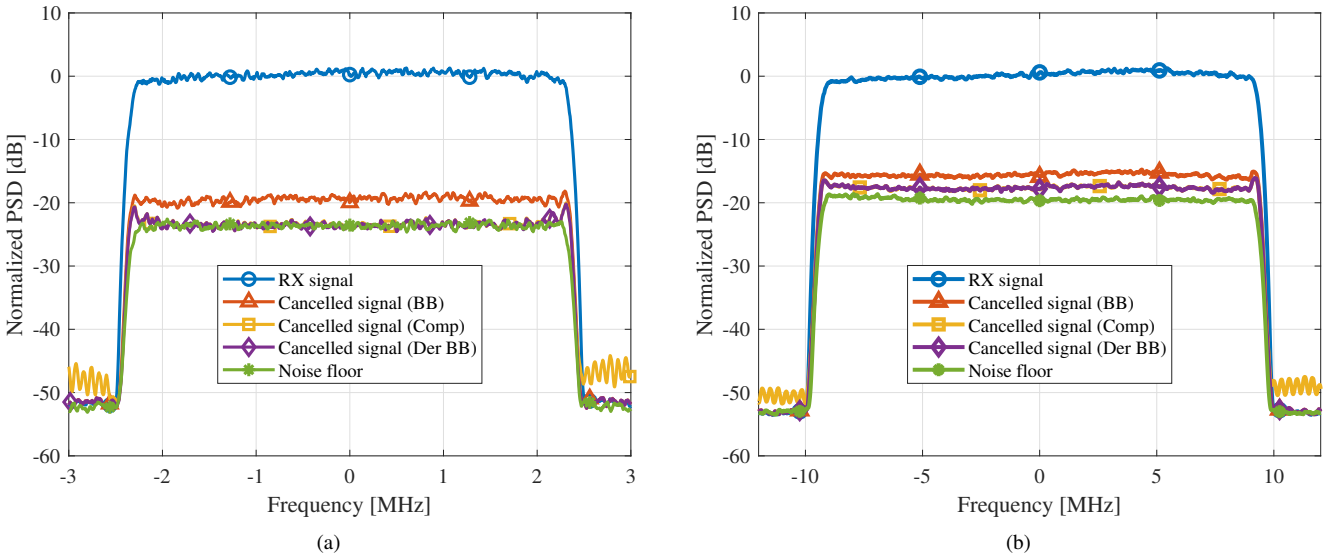

Fig. 5. Cancellation results with the three different cancellers utilizing (a) 5 MHz and (b) 20 MHz 5G NR compliant signals.

canceller $\mathbf{\Phi}_{\text{Der BB}}$ can be defined as

$$\mathbf{\Phi}_{\text{Der BB}}[t] = \left[\boldsymbol{\phi}_1[t+M_1] \ \cdots \ \boldsymbol{\phi}_1[t-M_2] \ \boldsymbol{\phi}_2[t+M_1] \ \cdots\right]. \tag{14}$$

where $\boldsymbol{\phi}_n[t]$ is the same as in (11), which does not require as high an oversampling as $\boldsymbol{\varphi}_p[t]$ in the Comp canceller.

For convenience, Table I collects the merits and drawbacks of each of the considered canceller solutions, that were discussed in this section. The main merit of the BB and Der BB cancellers is the lower required oversampling for the BF generation than the Comp canceller, which in turn generally requires less BFs per given BF order. Depending on the requirements of the target system, a suitable model can be chosen, based on the presented pros and cons.

IV. Measurements and Results

A set of measurements were conducted to verify the effectiveness of the canceller solutions. For this, a BS type system, consisting of a radio transceiver and directional antenna array is employed.

A. Measurement Setup

The measurement setup is shown in Fig. 4. The BS is placed in an anechoic chamber, with steel wool in the radiation field. Steel wool has been seen to function as a reliable, low cost source for PIM. The PIM source is placed 1.5 meters away from the BS and acts as the sole source of PIM in the test scenario, since the PIM levels generated by the BS system itself are insignificant. The BS is controlled via a PC from outside the chamber. The PC further collects data from the radio for postprocessing and PIM cancellation.

The measurements were conducted using random 5 MHz and 20 MHz 5G NR compliant OFDM signals. The TX power was set to +37 dBm, and the carriers were transmitted at frequencies 1819.0 MHz and 1866.5 MHz, which lie on the n3 band. The RX frequency then falls on 1771.5 MHz with 95 MHz separation, which is exactly the IMD3- frequency. The 5 MHz signal is natively sampled at 7.68 MHz and the 20 MHz signal at 30.72 MHz, and the composite signal is sampled at 122.88 MHz for the 5 MHz signals and 491.52 MHz for the 20 MHz signals. For comparison's sake, the cancellers employed similar parametrizations. Oversampling factor of 16 (compared to the native sampling rate) was used for the synchronization and BF generation tasks. The instantaneous BFs were used up to the fifth order, and the considered values for K were fixed at $\{-25,\ -9,\ 0,\ 9,\ 25\}$. Five taps of memory were applied, such that $M_1 = M_2 = 2$. With this parametrization, the BB and Der BB cancellers employ 75 BFs, while the Comp canceller employs 50. This parametrization is used for both 5 and 20 MHz signal cases.

B. Results with 5G NR Signals

Fig. 5(a) shows the cancellation results with the three canceller methods, utilizing pseudo-random 5 MHz 5G NR signals for transmission. The received signal, i.e., the PIM signal, is 23.9 dB above the noise floor, which is then the maximum observable PIM cancellation in this case. The BB canceller is able to cancel the PIM by 19.7 dB. The approximately 4 dB gap to the noise floor can be mainly explained by the lack of the TX path modeling, explained in the earlier section. In contrast, both the Comp and Der BB cancellers are able to push the residual PIM levels close to the noise floor, both achieving 23.7 dB of cancellation.

Finally, cancellation results of the cancellers when transmitting pseudo-random 20 MHz 5G NR signals are shown in Fig. 5(b). In this case, the received PIM signal is 19.7 dB above the noise floor, again setting the maximum achievable perceived cancellation at this level. Similar conclusions can

be drawn in this scenario as before: the BB canceller's performance is visibly hindered by the lack of TX chain modeling, achieving 15.9 dB of cancellation. Again, the Comp and Der BB cancellers outperform the BB one, both achieving 17.8 dB of PIM cancellation. The approximately 2 dB gap to the noise floor could be closed by considering higher order BFs and/or introducing more memory and envelope lead and lag terms, at the cost of adding more BFs to the system, thus increasing the computational complexity.

V. Conclusion

In this paper, we have considered air-induced PIM cancellation in FDD systems. We first introduced a system model in a case when air-induced PIM is perceived at the receiver. Stemming from the model, we obtain three canceller models, based on where the transmitted signal data is taken from in the TX chain. These canceller models were tested using measured data acquired from measurements conducted in an anechoic chamber. The more complicated Der BB and Comp cancellers were able to push the residual PIM levels close to noise floor, and it was noted that for higher modeling fidelity, the parametrization of the cancellers could be changed to consider higher order BFs and more memory and lead and lag in the envelope terms, at the expense of increasing the computational complexity. Overall, it was demonstrated that the air-induced PIM problem can be mitigated in FDD context using digital canceller solutions. In the future, the PIM issue could be investigated in a MIMO scenario, where more than two carriers are transmitted.

References

[1] 3GPP Tech. Spec. 38.104, "NR; Base Station (BS) radio transmission and reception," *v15.9.0, (Release 15)*, April 2020.

[2] A. Kiayani, M. Abdelaziz, L. Anttila, V. Lehtinen, and M. Valkama, "Digital Mitigation of Transmitter-Induced Receiver Desensitization in Carrier Aggregation FDD Transceivers," *IEEE Transactions on Microwave Theory and Techniques*, vol. 63, no. 11, pp. 3608–3623, 2015.

[3] J. J. Henrie, A. J. Christianson, and W. J. Chappell, "Linear–Nonlinear Interaction and Passive Intermodulation Distortion," *IEEE Transactions on Microwave Theory and Techniques*, vol. 58, no. 5, pp. 1230–1237, 2010.

[4] Q. Jin, J. Gao, G. T. Flowers, Y. Wu, and G. Xie, "Modeling of Passive Intermodulation With Electrical Contacts in Coaxial Connectors," *IEEE Transactions on Microwave Theory and Techniques*, vol. 66, no. 9, pp. 4007–4016, 2018.

[5] C. Yu, W. Cao, Y. Guo, and A. Zhu, "Digital Compensation for Transmitter Leakage in Non-Contiguous Carrier Aggregation Applications With FPGA Implementation," *IEEE Transactions on Microwave Theory and Techniques*, vol. 63, no. 12, pp. 4306–4318, 2015.

[6] A. Gebhard, O. Lang, M. Lunglmayr, C. Motz, R. S. Kanumalli, C. Auer, T. Paireder, M. Wagner, H. Pretl, and M. Huemer, "A Robust Nonlinear RLS Type Adaptive Filter for Second-Order-Intermodulation Distortion Cancellation in FDD LTE and 5G Direct Conversion Transceivers," *IEEE Transactions on Microwave Theory and Techniques*, vol. 67, no. 5, pp. 1946–1961, 2019.

[7] C. Motz, T. Paireder, and M. Huemer, "Low-Complex Digital Cancellation of Transmitter Harmonics in LTE-A/5G Transceivers," *IEEE Open Journal of the Communications Society*, vol. 2, pp. 948–963, 2021.

[8] M. Abdelaziz, L. Anttila, C. Tarver, K. Li, J. R. Cavallaro, and M. Valkama, "Low-Complexity Subband Digital Predistortion for Spurious Emission Suppression in Noncontiguous Spectrum Access," *IEEE Transactions on Microwave Theory and Techniques*, vol. 64, no. 11, pp. 3501–3517, 2016.

[9] H.-T. Dabag, H. Gheidi, S. Farsi, P. S. Gudem, and P. M. Asbeck, "All-Digital Cancellation Technique to Mitigate Receiver Desensitization in Uplink Carrier Aggregation in Cellular Handsets," *IEEE Transactions on Microwave Theory and Techniques*, vol. 61, no. 12, pp. 4754–4765, 2013.

[10] M. Z. Waheed, D. Korpi, L. Anttila, A. Kiayani, M. Kosunen, K. Stadius, P. P. Campo, M. Turunen, M. Allén, J. Ryynänen, and M. Valkama, "Passive Intermodulation in Simultaneous Transmit–Receive Systems: Modeling and Digital Cancellation Methods," *IEEE Transactions on Microwave Theory and Techniques*, vol. 68, no. 9, pp. 3633–3652, 2020.

[11] F. Kearney and S. Chen, "Passive intermodulation (PIM) effects in base stations: Understanding the challenges and solutions," *Visit analogdialogue. com*, p. 25, 2017.

[12] Z. Cao, F. Gao, X. Zhao, S. Zhang, K. Zhang, and Y. He, "Passive Intermodulation of Metallic Contact in Radiation Field," in *2019 IEEE 6th International Symposium on Electromagnetic Compatibility (ISEMC)*, 2019, pp. 1–4.

[13] T. Soares da Costa, "Characterization of Passive Intermodulation Distortion in MultiBand FDD Radio Systems," M.Sc. Thesis, KTH Royal Institute of Technology, Stockholm, Sweden, 2019.

[14] D. Morgan, Z. Ma, J. Kim, M. Zierdt, and J. Pastalan, "A Generalized Memory Polynomial Model for Digital Predistortion of RF Power Amplifiers," *IEEE Transactions on Signal Processing*, vol. 54, no. 10, pp. 3852–3860, Oct. 2006.